SASEC2015
Third Southern African Solar Energy Conference
11 – 13 May 2015
Kruger National Park, South Africa

PIN FIN TWO-PHASE MICROGAP COOLERS FOR CONCENTRATING PHOTOVOLTAIC ARRAYS

A. Reeser and A. Bar-Cohen
Department of Mechanical Engineering,
University of Maryland,
College Park, MD, USA
E-mail: alex.reeser@standardsolar.com
abc@umd.edu

G. Hetsroni and A. Mosyak
Department of Mechanical Engineering
Technion-Israel Institute of Technology
Haifa, Israel
E-mail: hetsroni@tx.technion.ac.il
mealbmo@tx.technion.ac.il

ABSTRACT:
Concentrating photovoltaic (CPV) systems are among the most promising renewable power generation options but will require aggressive thermal management to prevent elevated solar cell temperatures and to achieve the conversion efficiency, reliability, and cost needed to compete with alternative techniques. Two-phase, evaporative cooling of CPV modules has been shown to provide significant advantages relative to single-phase cooling but, to date, the available two-phase data has been insufficient for the design and optimization of such CPV systems.

This Keynote lecture will begin with a brief review of CPV technology and the solar cell cooling techniques described in the literature. Energy modeling, relating the harvested solar energy to the "parasitic" work expended to provide the requisite cooling, will be used to support the efficacy of two-phase cooling for CPV applications. Attention will then turn to the available correlations for pin-finned microgap coolers and the gaps which must be addressed to enable such thermal management for CPV arrays. This will be followed by a detailed description of an experimental study of 3 pin-finned microgap coolers for CPV systems and the derived heat transfer and pressure drop correlations. The data spans a large parametric range, with heat fluxes of 1 - 170 W/cm^2, mass fluxes of 10.7 - 1300 kg/m^2-s, subcooled (single phase) flow as well as exit qualities up to 90%, and 3 heat transfer fluids (water, HFC-134a, HFE-7200). The lecture will close with a brief case study of two-phase CPV cooling, demonstrating that the application of this thermal management mode can lead to a highly energy efficient CPV system.

INTRODUCTION:

Triple junction solar cells, made from horizontally stacked III-IV semiconductors, are a most promising alternative to silicon solar cells, with a conversion efficiency that has reached 44.7% with quad-junction cells [1] and is expected to reach even higher values over the coming years. The cell and layers are kept extremely thin – on the order of 8 μm for the top layers and 175 μm for the bottom substrate layer – to reduce internal series resistances and improve absorption and optical transmission. Each junction is tailored to a specific spectral range with minimal overlap, thereby capturing more of the solar spectrum than silicon and improving efficiency towards the theoretical maximum of 86.8% for an infinite-junction cell [2]. Although multi-junction III-V solar cells are more expensive than traditional crystalline silicon, the total cell area needed to provide a specified power level can be reduced, due to their inherently higher efficiency and the use of concentration, thus minimizing solar cell material cost. It is expected that concentrating photovoltaics (CPV), in which the large area of expensive semiconductors is replaced with an equivalent area of relatively low-cost optical reflectors, will lead to considerable cost savings. The power density per unit area of the cell is greatly enhanced by collecting and focusing the light into a small intense beam leading to a reduced cell footprint for comparable power generation. Because of this increased power density and reduced area, the cost of the highest efficiency cell can then be justified.

The magnification ratio or "suns" of a concentration system is the dimensionless unit by which solar concentrators are compared. It is defined as the ratio of average intensity of the focused light to the standard non-concentrated normal insolation, 1000 W/m^2 on the surface of the earth (e.g., 50 suns is 50 kW/m^2 of incident power). For high concentration systems of 500 suns or more, the most commonly used optics are point-focus parabolic dish mirrors or Fresnel lenses employed either as multiple, small one-cell systems in series-connected module arrays, or a densely packed "parquet" of cells with one large concentrator. Fresnel lenses function by focusing light via refraction and require a relatively short focal length which can be attained with comparatively less thickness

and less material than traditional convex lenses. Parabolic or circular paraboloid dish concentrators work by reflecting all incoming light incident on its surface to a single focal point, where the receiver containing the cells is located. Parabolic dishes can be scaled up or down in size and have a theoretical concentration limit of 10000 suns. This factor is lower in practice due to imperfections in the reflecting surface, but 2000 suns or more is attainable [3]. Some disadvantages of CPV systems that currently prevent widespread use are: dual axis tracking systems are required adding significantly to the system cost and complexity; optical concentrators do not work nearly as well with diffuse sunlight; and finally, high concentrations may necessitate the use of active cooling systems. Despite these limitations, CPV remain very promising for utility scale and high power installations.

Solar cells, like most semiconductor-based electronic devices,

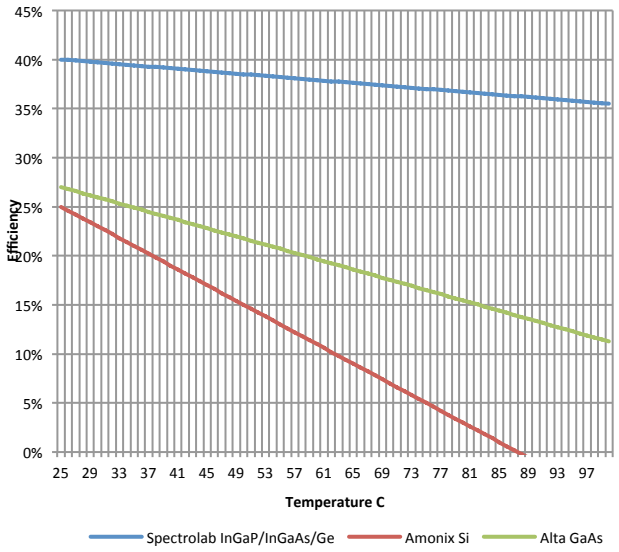

Figure 1: Comparison of three types of photovoltaic cells. Spectrolab InGaP/InGaAs/Ge triple junction, Amonix single junction Si, and Alta single junction GaAs **[6]**

are adversely affected by temperature. When the temperature rises more electrons are excited into the conduction band and, in a PV cell, this has the effect of reducing power conversion efficiency. The relationship of cell efficiency to temperature is commonly expressed as a simple, but useful linear equation which is expected to be quite accurate up to temperatures of about 350°C [4]. The efficiency quoted by manufacturers of solar cells is typically at ideal conditions, with the cell operating at 25°C in direct sunlight. Manufacturers will specify a mean value of the temperature coefficient for a large population of cells and a maximum continuous operating temperature, about 100°C for Spectrolab C4MJ cells [5]. It is to be noted that the temperature coefficient is difficult to measure, and can vary significantly depending on various parameters such as the type, diameter, thickness and configuration of the semiconductors used, the spectrum and concentration level of light in which it is being tested, and cell-to-cell manufacturing inconsistencies.

Figure 1 shows a comparison between production silicon, GaAs, and triple junction cells over a 25° - 100°C range [6]. It can be seen from the figure that the cell type and operating temperature can play an important role in cell efficiency and, hence, performance, especially at increasingly higher temperatures. The operating temperature of photovoltaic cells will always be above ambient without a cooling solution, due to the heat generated by the absorbed but "unconverted" incident sunlight. Cell to ambient temperature differences are typically 20°-30° with direct sunlight.

Despite the decreased conversion efficiency at elevated temperatures, it is unusual for non-concentrating solar cells to be actively cooled, due to the modest amounts of waste heat and the inability to recover the additional expense and parasitic cooling system power consumption of the cooling system. With increased concentration ratios the loss in efficiency becomes far more significant along with the risk of severe and permanent thermal degradation necessitating active thermal management for CPV systems.

Verlinden et al. [7] describes Solar Systems' production CPV system, based in Australia and capable of reaching 500 suns. It employs 40% efficient Spectrolab triple junction cells and uses an improved optical design with multiple reflecting mirrors assembled in a parabolic shape. The dish design allows the system to achieve a geometric concentration of 500 suns. A single array in one dish receiver consists of 64 "modules" and 1500 individual cells with module efficiencies as high as 36.1% and a total rated system output of 36.5kW per dish. A single-phase liquid cooling system is used [8] to remove the dissipated heat, requiring 950W, or less than 3% of total system output, to power the cooling system.

Currently, no production CPV systems are cooled using two phase flow and boiling. Although the technology has promise for CPV due to the low pumping power requirements and excellent heat transfer rates, the thermofluid transport mechanisms for flow boiling are not yet well understood. The only two-phase cooling photovoltaic study reported in the literature is by Ho et al. [8]. The authors analytically compared single phase water and two phase R134a for their high aspect ratio 1 m x 100 mm wide, single-channel cooler under 100 suns. They compared several flow rates, channel heights, and inlet temperatures and their effect on cell efficiency and performance. In the analysis they concluded that R134a was the superior fluid for two-phase cooling due to its low saturation temperature and low required pumping power.

As CPV concentrations begin to exceed 500 suns, heat fluxes are incident at the cell surface which cannot be easily removed with a 10-20C degree temperature rise. The need for area enhancement becomes more critical with these higher concentration ratios. Pin fin microgap coolers are an excellent

candidate to manage the higher heat fluxes generated by 500+ sun systems.

AVAILABLE HEAT TRANSFER CORRELATIONS

A summary of the best single phase micro pin fin correlation found in the literature for heat transfer coefficient and frictional pressure drop, proposed by Tullius et al. [9], is given in the following section. It was developed for a range of conditions, including various pin fin shapes, sizes and heat sink materials using water as the working fluid. It was found to have good prediction accuracy of 8%-9% MAE (depending on pin fin shape) for heat transfer coefficient and 6%-9% MAE for pressure drop (also depending on shape of the pin fins). The Tullius et al. correlation can be applied from micro- to mini-sized pin fins, as well as for a large range of heat flux (10–150 W/cm^2), mass flux (60 kg/m^{2}s–1000 kg/m^{2}s) and Reynolds numbers (100–1500). It is to be noted that successful correlation of the data, required a distinct geometric factor, $C_{Nu,}$ and $C_{f,}$ for each pin fin shape. The Tullius et al Nusselt number correlation for pin fins is given as:

$$Nu_f = C_{Nu}\left(\frac{S_L}{D_f}\right)^{0.2}\left(\frac{S_t}{D_f}\right)^{0.2}\left(\frac{h_f}{D_f}\right)^{0.25}\left(1+\frac{dh}{D_f}\right)^{0.4}\mathrm{Re}_f^{0.6}\mathrm{Pr}^{0.36}\left(\frac{\mathrm{Pr}}{\mathrm{Pr}_s}\right)^{0.25} \quad (1)$$

Geometry	Circle	Square	Diamond	Triangle	Ellipse	Hexagon
C_{Nu}	0.08	0.0937	0.036	0.0454	0.0936	0.0752

For frictional pressure drop, Tullius et al used a similar correlational form along with a shape multiplier as below:

$$f = C_f\left(\frac{S_L}{D_f}\right)^{0.2}\left(\frac{S_t}{D_f}\right)^{0.2}\left(\frac{h_f}{D_f}\right)^{0.18}\left(1+\frac{dh}{D_f}\right)^{0.2}\mathrm{Re}_f^{-0.435} \quad (2)$$

Geometry	Circle	Square	Diamond	Triangle	Ellipse	Hexagon
C_f	2.96	5.28	1.81	2.45	3.44	4.53

The summary of all the two-phase micro pin fin correlations, used in this work for the heat transfer coefficients and frictional pressure drop, are given below. All the two-phase micro pin fin heat transfer correlations found in the literature were developed for highly subcooled inlet conditions and low exit thermodynamic vapor qualities. No studies (at the time of this work) exist for saturated or near saturated inlet conditions nor for high vapor quality flow conditions.

The correlation for heat transfer coefficient by Krishnamurthy and Peles [10] was developed for high heat flux cooling (20–350 W/cm^2) with a silicon pin fin microcooler, having circular staggered pin fins of 100μm diameter. It uses a superposition type model, with the nucleate boiling term removed. The single-phase Nusselt number relation is believed to be valid for Reynolds Numbers less than 10^3. The correlation is given in Equation 3 as follows:

$$h_{tp} = \zeta\left(\phi^2\right)^{0.2475} h_{sp} \quad (3)$$

$$h_{sp} = \frac{Nu \cdot k_f}{d_{fin}}$$

$$Nu = 0.76\left(\frac{S_t}{d}\right)^{0.16}\left(\frac{S_L}{d}\right)^{0.2}\left(\frac{H_{fin}}{d}\right)^{-0.11}\mathrm{Re}^{0.33}\mathrm{Pr}^{0.333}$$

$$\left(\phi\right)^2 = 1+\frac{0.24}{X_{vv}}+\frac{1}{X_{vv}^2} \qquad \zeta = 1$$

$$X_{vv} = \left[\frac{\left(\Delta P_f/\Delta Z\right)_f}{\left(\Delta P_f/\Delta Z\right)_v}\right]^{1/2} \qquad \left(\Delta P_f\right)_f = \frac{fN\left(G\left(1-x\right)\right)^2}{2\rho_f}$$

$$\left(\Delta P_f\right)_v = \frac{fN\left(Gx\right)^2}{2\rho_v}$$

In Equation 3, X_{vv} is the Martinelli parameter, N is the number of pin fin rows in the flow direction, f is the single phase friction factor, x is the exit quality, S_t, S_L and H_{fin} are the transverse, longitudinal and height of the fins respectively.

The Qu and Siu-Ho [11] correlation was developed for high heat flux cooling (25 – 250 W/cm^2) utilizing a square, staggered copper pin fin array with a subcooled inlet. The model was fitted to Qu and Siu-Ho's original data and requires a subcooling term, in the form of negative inlet quality, in order to obtain proper results. It is, therefore, not applicable to a fully saturated inlet condition, but is presented below for completeness:

$$h_{tp} = 1.0 - 12.2 \cdot x_{in}\exp\left[-(101 \cdot x_{in} + 29.4) \cdot x_e\right] \cdot 50.44 \quad (4)$$

where x_{in} is the inlet subcooling and x_e is the local quality.

The heat transfer coefficient model developed by McNeil et al. [12] is for relatively low heat flux cooling (1 – 15 W/cm^2) using refrigerant R113 in copper inline pin fins. Similar to the Krishnamurthy and Peles model, it utilizes superposition, which addresses the nucleate boiling and convective heat transfer mechanisms separately. It is the only micro pin fin correlation in this study that was developed for two phase inline pin fin arrays. The correlation is given below.

$$h_{tp} = S \cdot h_{nb} + F \cdot h_{conv} \quad (5)$$

In the McNeil et al correlation the single-phase convective term is given as:

$$h_{sp} = \frac{Nu \cdot k_f}{d_{fin}}$$

$Nu = Nu_r \times F_1 \times F_4$ (F_4 *is a row dependent multiplier*)

$Nu_r = a \cdot \mathrm{Re}_b^m \, \mathrm{Pr}_b^{0.34}$

For $\mathrm{Re} < 300$, $a = 0.742, m = 0.431$

For $300 < \mathrm{Re} < 2\times10^5$, $a = 0.211, m = 0.651$

For $\mathrm{Re} > 2\times10^5$, $a = 0.116, m = 0.7$

$$F_1 = \left(\frac{\mathrm{Pr}_b}{\mathrm{Pr}_w}\right)^{0.26}$$

The nucleate boiling term in the McNeil et al correlation is expressed in terms of the reduced pressure, P_r, as:

$$P_r = \frac{P}{P_{cr}}$$

$$h_{nb} = 0.945P_r^{0.17} + 4P_r^{1.2} + 10P_r^{10}(P_{cr}/1000)^{0.69}(q''/1000)^{0.7}$$

The Enhancement and Suppression factors for Eq. 5 are given by:

$$X_0 = 0.041\left[\frac{\sigma}{g(\rho_l - \rho_v)}\right]^{1/2} \qquad F = \left(\phi_L^2\right)^{0.36}$$

$$X_c = F \cdot h_{conv}\frac{X_0}{k} \qquad (\phi_L)^2 = 1 + \frac{8}{X_{tt}} + \frac{1}{X_{tt}^2}$$

$$S = \frac{1}{X_c}\left(1 - e^{-X_c}\right) \qquad X_{tt} = \left(\frac{1-x}{x}\right)^{0.9} * \left(\frac{\rho_v}{\rho_l}\right)^{1/2}\left(\frac{\mu_l}{\mu_v}\right)^{0.1}$$

DESCRIPTION OF THE EXPERIMENTAL APPARATUSES

In the present work, two separate Copper micro pin fin arrays of staggered and inline configuration were manufactured on equal overall base areas as well as equal pin width and height, so that performance between the two arrays may be directly compared. In this section, a detailed overview of the testing loop and experimental procedure used to evaluate the thermofluid performance of these micro pin fin channels are discussed.

Test Loop: The following devices were used in the experiment: the micro pin fin test section, liquid-cooled condenser, liquid reservoir, fluid pump, rotameter, two inline heaters, inlet and outlet pressure transducers, and various E-type thermocouples for reading fluid and test section temperatures. Semi-transparent, high temperature, flexible silicone rubber tubing were used to connect these devices and

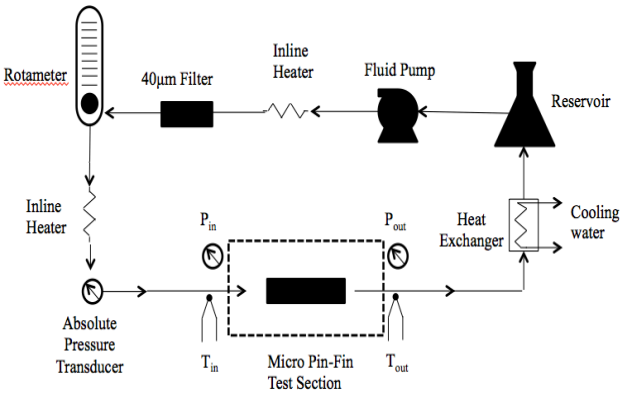

Figure 2: Micro-pin-fin testing loop

provided a robust and easily customizable test vehicle for the current set-up.

A schematic of the testing loop is shown in Figure 2. For pressure readings, two separate transducers were used, one at the inlet and one at the outlet, so that inlet and outlet pressures could be measured independently. This was done to enable determination of the liquid subcooling, confirmation of saturated boiling condition, and the vapor quality at the exit, along with temperature readings. Two inline heaters were used to heat the fluid to the desired inlet temperature, with sufficiently low power in each heater to avoid premature boiling or liquid dryout inside the heaters before reaching the test section. A McMaster-Carr 40μm inline filter was inserted upstream of the test section to prevent contaminants from clogging the micro pin fins. The rotameter is an Omega FL-5000 series flow meter with interchangeable tubes. It was installed with a 305cc/minute maximum flow rate tube with 150mm markings. Flow readings are measured visually with the metal ball float, and flow rate can be controlled with the integrated valve. The condenser is a flat plate heat exchanger, cooled with forced convection water. The flow rate of the cooling water was manually controlled to condense the working fluid and lower the working fluid temperature to the desired value before entering the reservoir. The pressure transducers were Setra Systems Model 230 with voltage signals between 0.05 and 5.05V. The pressure range for each

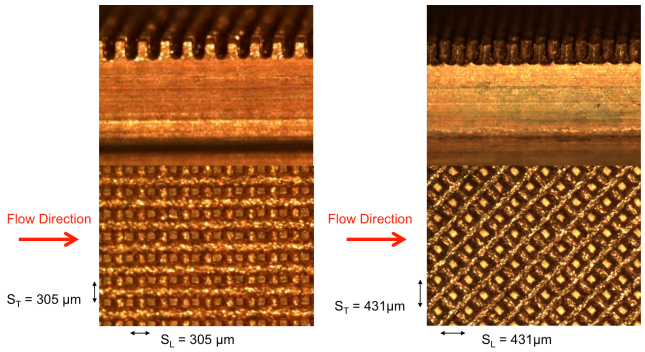

Figure 3: Inline and Staggered Pin Fin Arrays

sensor was 0 – 50psi and 0 – 5psi, for the inlet and outlet sensor respectively. An absolute pressure transducer was used to verify the inlet pressure reading.

Pin Fin Arrays: Two micro pin-fin arrays, a staggered configuration and inline configuration, were fabricated out of Copper, using a wire electric discharge machining (EDM) process. The arrays had equivalent base areas of 0.96cm x 2.88cm and used identical square pin fin width and height of 153μm and 305μm, respectively, to allow for direct performance comparisons. Due to their orientation, the inline and staggered arrays differ in their transverse and longitudinal spacing, with both dimensions equaling 305μm for the inline array, while both spacings equaled 431μm for the staggered array. Figure 3 contains a side-by-side visual comparison of these two arrays.

Three, approximately 1 cm^2 square ceramic heaters were soldered on the back of each array, using 63% Sn/37% Pb electronic grade solder paste. Ten small holes were drilled above the heated surface where thermocouples were inserted to measure the wall temperature of the test section. One polycarbonate (Lexan) housing was manufactured to fully enclose the pin fin array being tested, while providing insulation from natural convection heat losses during testing. The housing and pin fin arrays were designed such that easy replacement of test sections could be accomplished as needed with no other modification to the testing loop. On top of the housing, a polycarbonate cover was attached and sealed with silicone RTV. Figure 4 is an exploded view of the full assembly.

Test Procedure: The procedure to obtain single phase data was as follows: the flow rate was set to the desired value using the rotameter. Next the inline preheaters were turned on and set to a power that would yield the inlet temperature for the tests. The heat exchanger cooling water flow was then turned on. A low initial heating level was applied at the test section, using the power supply. Heat was increased in small increments for each test and the system was allowed to reach steady state, which took about 2-3 minutes, before data readings were gathered. The procedure to gather two phase data was similar to the single phase procedure. After all tests with water were completed, the testing loop was drained of all fluid and allowed to dry for several days. Afterward, the testing loop was charged with HFE-7200 and similar testing procedures to water were performed. Two runs of each mass flux for staggered and inline were run with repeatability in the range of 2% - 5%.

Additional experiments were performed using a similar micro-pin fin heat sink designed by David et al. [13]. The heat sink was fabricated of copper, again using the electric discharge machining method. Silver over nickel plating was applied to the heat sink to allow soldering of the resistor to the heat sink base with overall dimensions of 1×1 cm^2. The pin-fins are 0.35×0.35 mm in diameter, 1 mm in height, and have a pitch of 0.45 mm. The dimensions were chosen based on typical micro-scale devices described in the literature. To minimize the pressure drop the pin-fins were designed in staggered arrangement, with pin-fin corner normal to the flow direction.

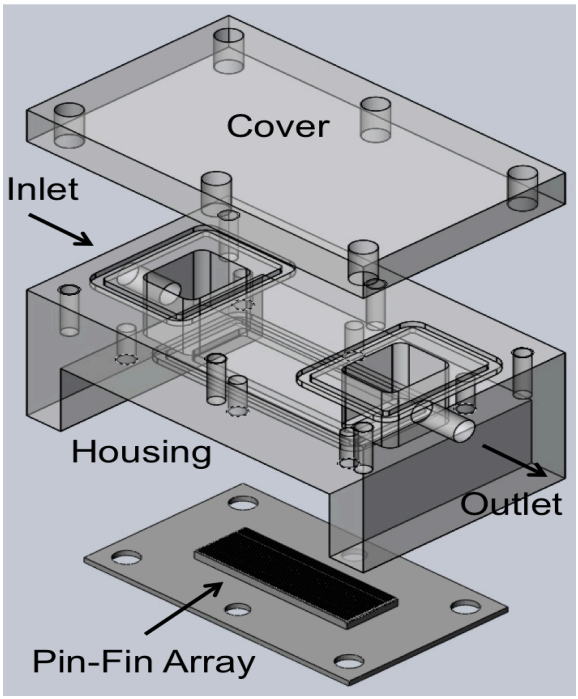

Figure 4: Exploded view of test section

SINGLE PHASE MICRO PIN FIN EXPERIMENTS

Single phase experiments were performed with deionized water and HFE-7200 in both the staggered and inline arrays. The tests established a baseline to which the available correlation could be compared, as well as to gauge the relative cooling performance enhancement for the two phase flow boiling experiments. Inlet temperature for all single phase experiments was held constant at 30°C. Plots of single phase average heat transfer coefficient versus heat flux for both deionized water and HFE-7200, in the in-line and staggered arrays, are given in this section. Results were corrected for fin efficiency, and the average heat transfer coefficient is based on the total wetted area of the channel. In Figure 5, the results for deionized water in the in-line array and staggered array are shown for 4 different mass fluxes from 400 kg/m^2s to 1300 kg/m^2s (calculated using the open area at the entrance to the test section) and heat fluxes in the range of 10 to 110 W/cm^2. A detailed error analysis suggests that the measured values are within the +/-16% error bars shown in the Figures.

It can be seen that while the average heat transfer coefficient is almost independent of heat flux (zero slope) for a constant flow rate, a 3x increase of mass flux will cause the average heat transfer coefficient to increase by about 2x. Additionally, it can be seen that the heat transfer coefficients for the in-line and staggered arrays are similar in magnitude for equivalent mass fluxes, with the inline array slightly better, except for the highest mass flux of 1300 kg/m^2s.

The Tullius et al. correlation prediction as published for the inline and staggered arrays provides square and diamond shape factor multipliers of 0.0937 and 0.036 respectively. Using these values significant mean average errors (MAE) of 87.52% are found between the correlation and the inline array data. However since the correlation was developed exclusively from staggered array data the UMD inline array is outside the parametric range of the Tullius correlation - far lower MAE of 16.09% was found for the staggered array. Since the current data is within the parametric range of Tullius et al., higher accuracy is anticipated for the staggered configuration but the agreement between the data and the correlation is still not as good as the MAE of 9% reported by Tullius et al. Interestingly the accuracy of the correlation can be improved to MAE of 3.48% for the inline array by altering the shape factor to 0.0495, and an MAE of 12.07% for the staggered array by altering the shape factor to 0.0413. The comparison of the modified Tullius et al. correlations and the UMD single phase data is shown in Fig 5. It is to be noted that the selected shape factors are within range of the published shape factors values, as stated above.

The results for HFE-7200 average heat transfer coefficient versus heat flux for the in-line and staggered arrays are shown in Figure 6 for 3 different mass fluxes from 200 kg/m^{2}s to 600 kg/m^{2}s, with an expected experimental discrepancy of ±16%. Similar to water, a 2x improvement in the average heat transfer coefficient occurs for a 3x increase in mass flux. The magnitude of the heat transfer coefficients is lower than for water due to HFE-7200's relatively poor convective thermal properties. It may also be noted that the HFE data display a somewhat stronger dependence on heat flux than seen in the single phase water data. At the same mass flux the staggered array was found to provide 30%-50% higher heat transfer coefficients than the in-line arrays, for the two highest mass fluxes. Additionally, a nearly 3x improvement in the average heat transfer coefficient occurs for a 3x increase mass flux and the heat transfer coefficient appears to display a more complex dependence on heat flux than seen with water. Relatively high MAE values were found between the Tullius et al. correlation and data, reaching 70.47% overall for the inline array and 36.49% for the staggered array. As seen in Figure 6, displaying the measured UMD data and the modified Tullius et al. correlation, the accuracy of the correlation can be improved to 9.28% for the inline array by setting the shape factor to 0.054, and to 23.35% for the staggered array by setting the shape factor to 0.065. While these shape factors differ from the values proposed by Tullius et al. for the square and diamond shaped pins, with 0.0937 and 0.036, respectively, they do fall within the stated range of these shape factors.

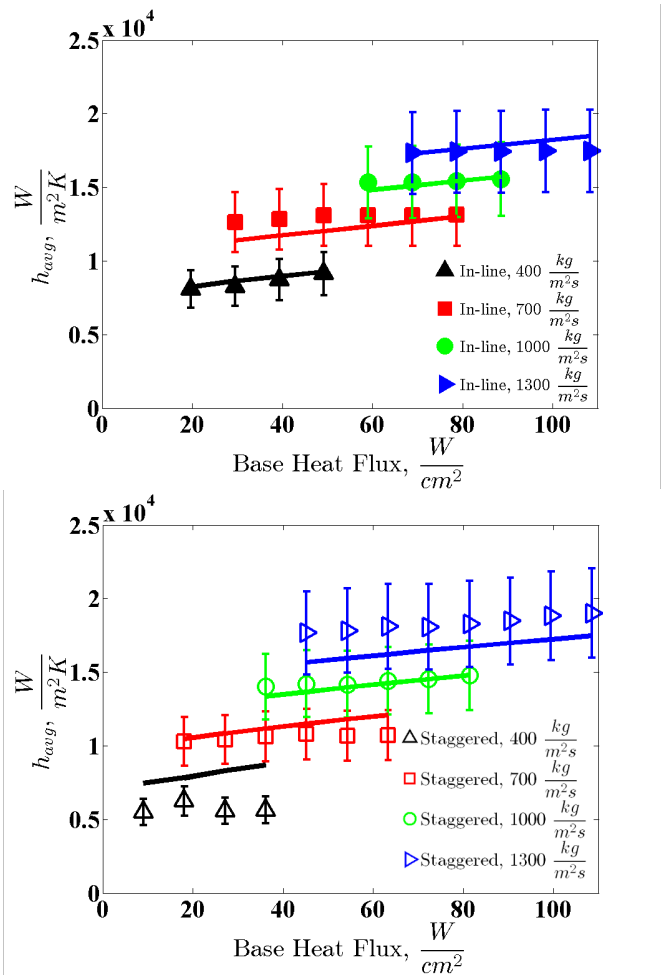

Figure 5: Modified Tullius et al. prediction for single phase water in the inline array (top) using a 0.0495 shape factor and the staggered array (bottom) using a 0.0413 shape factor.

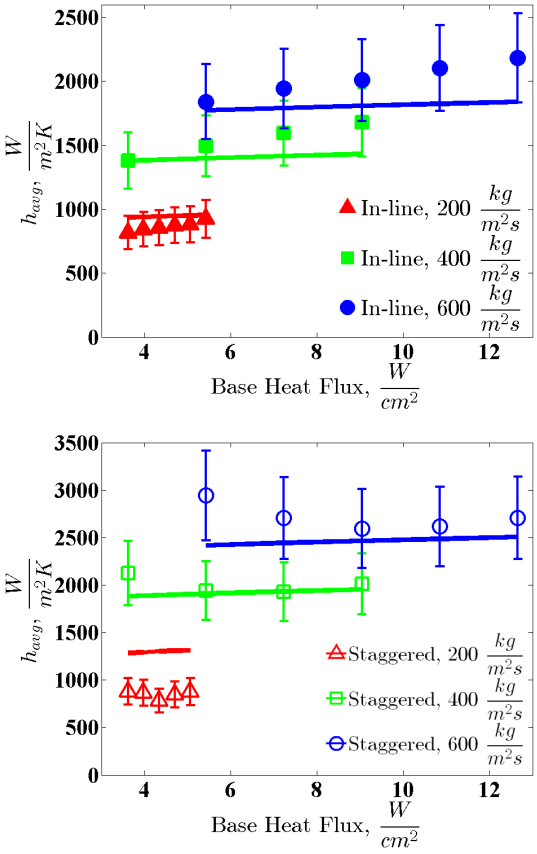

Figure 6: Modified Tullius et al. prediction for single phase HFE-7200 in the inline array (top) using a 0.054 shape factor and the staggered array (bottom) using a 0.065 shape factor.

For the additional heat sink in [13] experiments were performed in the range of heat flux q=5.2-24.7 W/cm^2 and mass flux G=10.7-39.1 kg/m^{2}s. A thermal high speed imaging radiometer was utilized to study the temperature field on the electrical heater. We compared temperature non uniformity (on the heated surface) under conditions of convective heat transfer of water in micro-channel without pin-fins.

The temperature distribution on the heated wall depends on the material and design of the test module, flow rate in the micro-channel, heat flux, and type of working fluid. The infrared image and histogram of the temperature distribution on the heated side of the test module is shown in Figs. 7a and 7b at m=34.5 kg/ m^{2}s, q=16.0 W/cm^2.

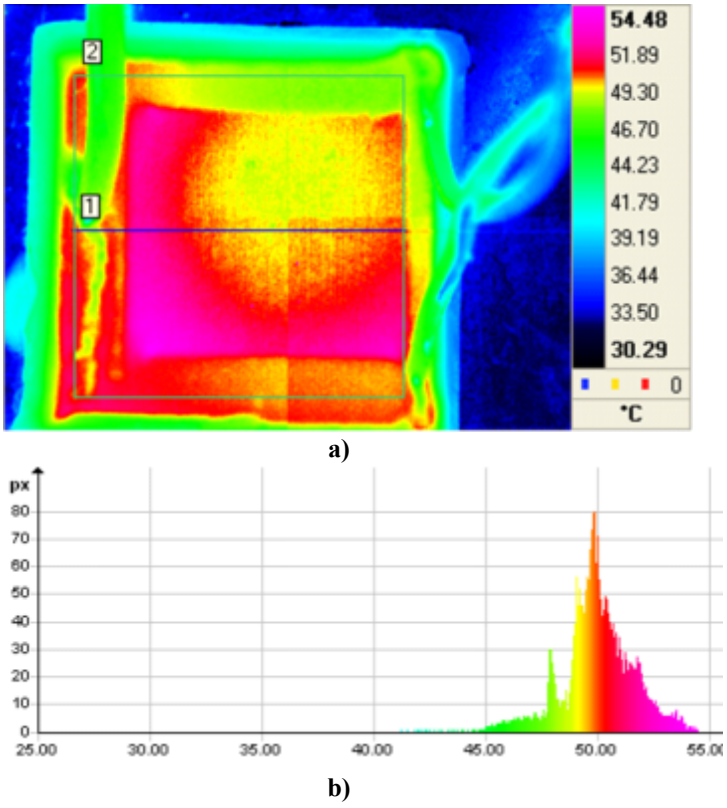

Figure 7: Temperature distribution (T_W) on the whole heated surface (marked as the square 2) at G= 34.5 kg/m^{2}s, q= 16.0 W/cm^2

The flow is from the left to the right. The area of the heater (the marked square 2) is clearly shown, and the thermal image analysis is restricted to this square area of 9.5 × 9.5 mm^2. As can be seen from the histogram, the temperature of the resistor was mainly concentrated around 50 ºC and did not deviate much from this value. Figures 8a and 8b show temperature distribution (line 1) on the center of heated surface in the flow direction at m=22.2 kg/m^{2}s, q=11.6 W/cm^2 and m=34.5 kg/ m^{2}s, q=16.0 W/cm^2. Though the graphs do not display a constant temperature, they have temperature fluctuations with small values of standard deviation. It may be concluded that the temperature distribution across the resistor in the direction of flow is nearly uniform. Comparison of temperature distribution between pin-fin

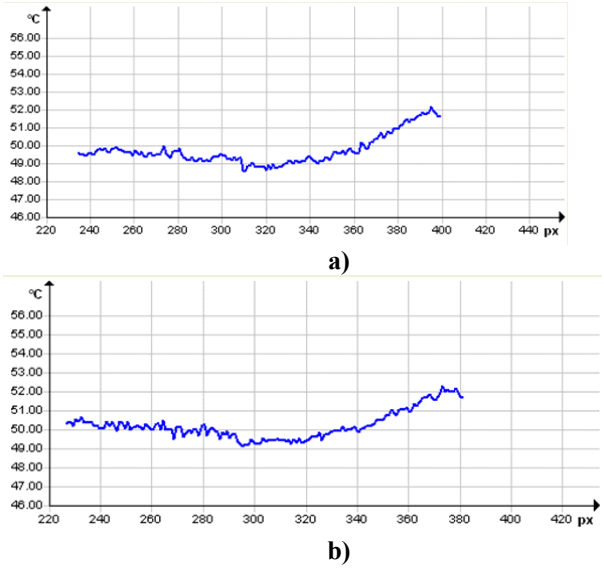

Figure 8: Temperature distribution (T_W) on the whole heated surface (marked as the square 2) at G= 34.5 kg/m^{2}s, q= 16.0 W/cm^2

and smooth micro-channels at the same mass flux and heat flux conditions is shown in Figs. 9a and 9b. The heat transfer coefficient in smooth micro-channel was calculated using theoretical value of the Nusselt number Nu=4.36. It is not depend on mass flux. In the pin-fin het sink the heat transfer coefficient increases along the flow direction. When a fluid flows across pin-fins, centrifugal forces cause secondary fluid motion, which gives rise to increased heat transfer rates. At very short distances from the start of heat transfer zone, the thermal boundary layer near the base of heat sink is to thin to be affected by secondary flow field. Therefore near the inlet pin fins offer a little advantage over a straight micro-channel.

For greater axial distances the enhancement factor increases. It should be noted that the smooth micro-channels follow an established relationship in which the temperature of the fluid changes linearly in the flow direction and that the temperature of the item being cooled follows this same linear rate of change but at higher temperatures. From Figs. 9a and 9b one can see that the use of a micro-channel with micro-pin fins results in more uniform temperature distribution as compared to smooth micro-channels.

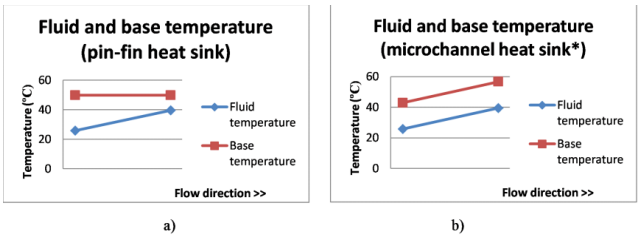

Figure 9: Comparison between temperatures on the heated wall, G=34.5 kg/m^{2}s, q=16.0 W/cm^2 a) micro-channel with pin fins, b) smooth micro-channel

Temperature measurement results: Figure 10 depicts the average temperature, T_W, of the heater, as measured with the radiometer . It shows the variation of T_W with q at three values of mass flux, G. At all values of mass flux T_W decreases with increasing G for a given q. At given mass flux, T_W increases linearly with increasing the heat flux. The overall trend in the measured wall temperature is typical of a single-phase heat transfer system. It should be stressed that local temperatures of the heater in the present experiments are very close to T_W.

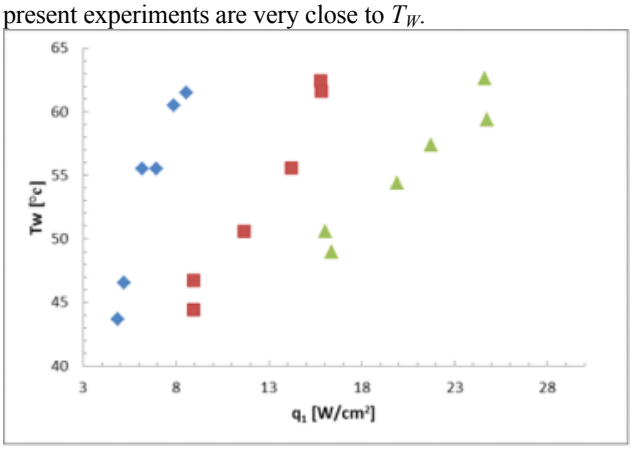

Figure 10: Variation of the average wall temperature measured by IR with input heat flux.
◊- G=11.6 kg/m2s , □- G=23.8 kg/m2s , Δ- G=36.8 kg/m2s

One drawback of a micro-channel heat sink with single-phase cooling is a relatively high temperature rise along the micro-channels comparing to that for traditional heat sink designs. In the micro-channel heat sink, the large amount of heat generated by high concentrator photo-voltaic system is carried out from the package by relatively small amount of coolant. Large temperature rise produces thermal stresses in elements and packages due to the differences in the coefficient of thermal expansion, thus undermining the devices reliability. This temperature rise may be accompanied by a complex pattern of spatial temperature variations that can produce potentially destructive thermal stresses along the interface between the solar cell and the heat sink. This is one of the key justifications for seeking a nearly isothermal heat sink. Furthermore, a large temperature gradient is undesirable for the performance of the photo-voltaic cells since many electronic parameters are adversely affected by substantial temperature gradients. For instance, electrical-thermal instability occurs within a high temperature region, because the base elements of photo-voltaic cells have a switching time that decrease with increasing temperature. In the present experiments (the range of heat flux q=5.2-24.7 W/cm^2 and mass flow rate m=0.062-0.23 g/s) for cooling by very small amount of coolant using pin-fin micro-heat sink the temperature distribution on the whole heater recorded by IR camera showed that the standard deviation from the average temperature of the heated wall is 0.3-1.9 K and the maximum difference of the wall temperature between different points does not exceed 3-5 K.

TWO PHASE MICRO PIN-FIN EXPERIMENTS

Two phase flow boiling experiments were performed with deionized water and HFE-7200 in both the staggered and inline arrays. The goals of the experiments were to evaluate the cooling enhancement that two phase flow boiling could provide over the single phase baseline and to determine the accuracy of the existing two phase correlations for prediction at high exit qualities. The results would support the determination of the best pin fin configuration for energy efficient cooling at the high heat fluxes that are encountered in a CPV array. In the following sections, the two phase cooling experiments are described along with a comparison of the results to those available in the existing literature. Plots of two phase average heat transfer coefficient versus exit quality for both deionized water and HFE-7200, in the in-line and staggered arrays, are given in this section. Results were corrected for fin efficiency, and the average heat transfer coefficient is based on the total wetted area of the channel.

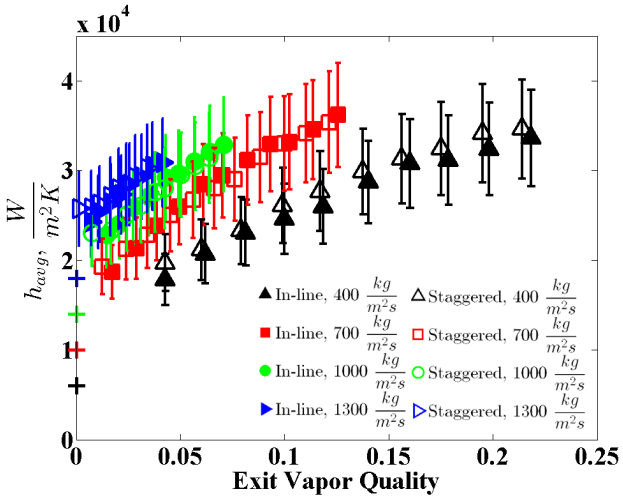

Figure 11: Average two phase heat transfer coefficient versus exit quality for water in the staggered and inline pin fin arrays. Error bars indicate

Water entered the test sections at about 95°C, keeping the subcooling low so as to subsequently allow exit qualities to be as high as possible, while keeping surface temperatures below 140°C to prevent thermal destruction of the test apparatus or any of the components. Figure 11 is a plot of the two phase water average heat transfer coefficient versus exit quality for the inline and staggered arrays for 4 different mass fluxes from 400 kg/m^{2}s to 1300 kg/m^{2}s and heat flux from 27 W/cm^2 to 118 W/cm^2. The expected experimental uncertainty of ±16% is indicated by the error bars

Distinct trends can be observed for each mass flux, with the heat transfer coefficient at the same exit quality increasing with mass flux. As the exit quality increases, the average heat transfer coefficient also monotonically increases, with all data points better than the respective single phase asymptote marked on the y-axis as 0% exit quality. It is also important to note that the inline and staggered data points nearly coincide over the entire range of qualities shown here, implying that neither the inline nor staggered array is significantly better than the other in terms of cooling performance.

Comparison of the current water data with the available two phase correlations outlined in Chapter 1 reveal the large differences in the trend and magnitude of the predicted heat transfer coefficients among these correlations. While the heat transfer coefficients are observed to generally increase with exit quality in this parametric range, the Qu and Siu-Ho correlation displays a nearly "quality-independent" behavior with a slight downward trend of the heat transfer coefficients with quality, having an MAE of 118% for inline and 129% for staggered. Parametrically, working fluid, heat fluxes, mass fluxes along with Prandtl and Reynolds number are within range of the Qu and Siu-Ho correlation, however their high inlet subcooling and staggered square pin fin geometry is substantially different from the current pin fin array experiments. The McNeil et al. correlation has a trend similar to the data but substantially overpredicts the empirical results with an MAE of 363% for inline and 351% for staggered. The overprediction by McNeil et al. could be explained by, not only the larger 1mm x 1mm pin fins used in their experiments, but also the R113 refrigerant working fluid that was used. The correlation with the best overall prediction capability for these empirical results is by Krishnamurthy and Peles with an MAE of 109% for inline and 144% for the staggered configuration. Once more, similar geometric deviations occur with the circular, staggered pin fin array used for the Krishnamurthy and Peles correlation. Additionally, the inlet subcooling was much higher than for the current work. These discrepancies are substantially beyond the ±16% measurement error and cannot be explained by experimental uncertainty alone.

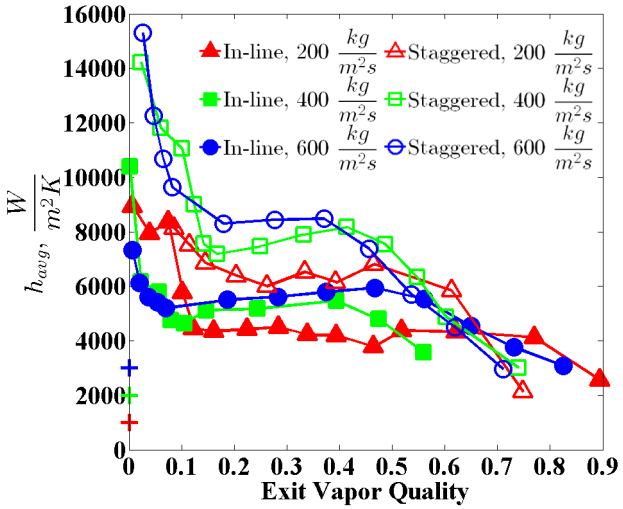

Figure 12: Average heat transfer coefficient vs. exit quality for two phase HFE-7200 in the inline and staggered arrays. "+" markings indicate single phase asymptotes.

HFE-7200, with a boiling point of 76°C at atmospheric pressure, entered the pin fin array at 70°C, keeping the level of subcooling low to allow the exit qualities to be as high as possible. The same 3 mass fluxes of 200 kg/m^{2}s, 400 kg/m^{2}s and 600 kg/m^{2}s, studied in the single phase HFE-7200 experiments, were chosen for the two-phase experiments. Heat fluxes ranged from 1 W/cm^2 to 36 W/cm^2. Due to the low latent heat of the HFE-7200, the experiments spanned a broader range of exit qualities, exceeding 70% for all the experiments and reaching a maximum value of 90% for the in-line pin fin array operating at a 200kg/m^{2}s mass flux.

Inspection of Figure 12 immediately reveals distinct differences between the two phase HFE-7200 heat transfer coefficients and the water data in Figure 11. Unlike the observed behavior with water, the HFE-7200 data reveals an approximately 50% improvement in the average heat transfer coefficient of the staggered array over the inline array, for much of the range of exit qualities. Most notable for both HFE-7200 array configurations is the initial sharp decline in the average heat transfer coefficient from the lowest exit qualities to about 10% - 15% followed by a plateauing or mild increase up to exit qualities of 40% - 50% where it reaches a local maximum. Finally, the average heat transfer coefficient deteriorates as the exit quality approaches 100%, possibly reflecting localized dryout in the pin fin array. It should be noted that the two phase heat transfer coefficients exceed that of the single phase asymptote ("+" markings on plot) over the entire exit quality range, for all mass fluxes. It is to be noted that the ±16% measurement error bars were left out of Figure 12 for clarity.

As expected there is significant disagreement between the two phase correlations in the literature and the HFE-7200 data. Especially of note is the multiple inflection points of the average heat transfer coefficient over exit quality which are not readily captured by 2 of the 3 available correlations. The Qu and Siu-Ho correlation in general overpredicts with an MAE of 110.4% for the inline array and 59.32% for the staggered array. The Krishnamurthy and Peles correlation fails to capture the trend of the heat transfer coefficient with exit quality for HFE-7200, but has an overall MAE of 87.5% for the inline array and 93.6% for the staggered array. Since none of the available correlations were developed for HFE-7200, it is expected that they would not predict the current data well. In addition to the geometrical deviation of the current pin fin arrays to each of the correlations as mentioned in the previous section for water, the heat fluxes for HFE-7200 are particularly low for both arrays and out of the range of the correlations. Additionally, the exit qualities in the current HFE-7200 data substantially exceeded the maximum observed for any of the literature from which these correlations were borrowed. The maximum observed exit quality was in Qu and Siu-Ho and was 26%.

The observed variation of the heat transfer coefficient with quality is reminiscent of the trends described previously in microgap flow boiling experiments by Rahim et al. [14] Though it was suggested by Krishnamurthy and Peles that there may be flow regimes unique to micro pin fin arrays, such as bridge-flow [10], the observed trend in this study is analogous to that occurring in microgaps and microchannels, and may thus be explained by the general physics of two phase phenomena in microchannels. Following Rahim et al [14], it can be expected that two-phase heat transfer coefficients will increase steeply from their single-phase values upon the initiation of nucleate boiling, for incrementally positive flow qualities, then decrease by transition to intermittent flow, as vapor "slugs" pass through the pin fin array and induce portions of alternating thin film evaporation and local dryout at the wall and surrounding pin fins. As the end of the slug-vapor intermittent regime and the onset of annular flow is approached, the heat transfer coefficient can be expected to plateau and then begin to increase as thin film evaporation becomes the dominant heat transfer mechanism and rising heat transfer coefficients result from thinning of the evaporating liquid film surrounding the pin fins. Farther into the annular regime, a decrease in the heat transfer

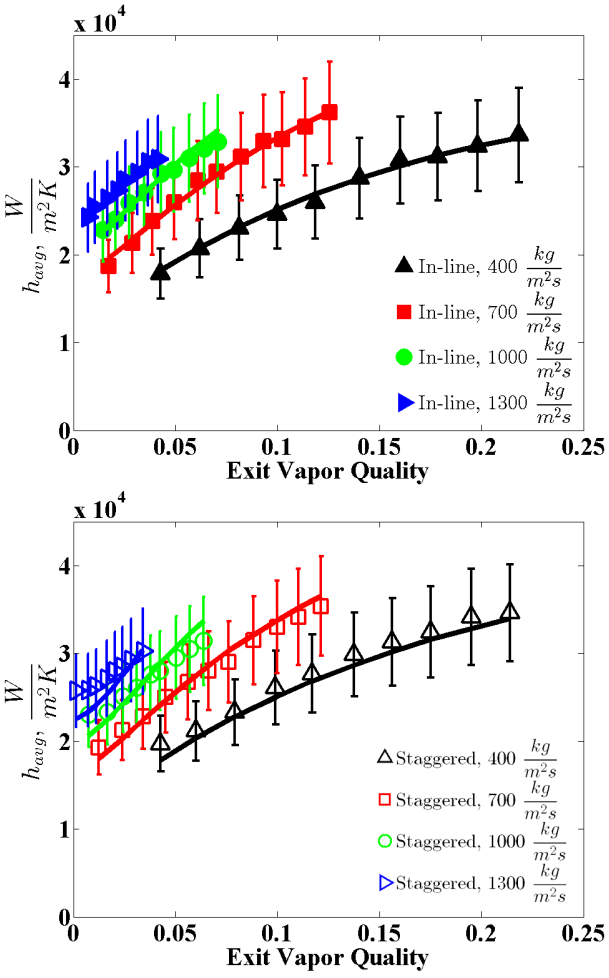

Figure 13: New two phase heat transfer coefficient correlation prediction for water in the inline array (top) and staggered array (bottom)

coefficient occurs, resulting from widespread local dryout of the liquid film. While the exact flow regime progression for

pin fin microchannels is as yet unknown, the similarity of the observed variation in the heat transfer coefficient with exit quality to that seen in microgap channels provides an initial basis for interpreting these empirical results.

As described in the current chapter, correlations available in the literature are unable to predict the current two phase heat transfer coefficient data, especially over the broad range of exit qualities that were investigated. Therefore it is important to develop a robust new correlation that can predict the performance of the inline and staggered arrays for both water and HFE-7200 with low average error. Since the Krishnamurthy and Peles correlation had the best overall performance, we will start with the same form they developed and make a few key changes to improve it. First, the Nusselt number correlation by Short et al. used by Krishnamurthy and Peles was originally developed for large, air-cooled pin fin

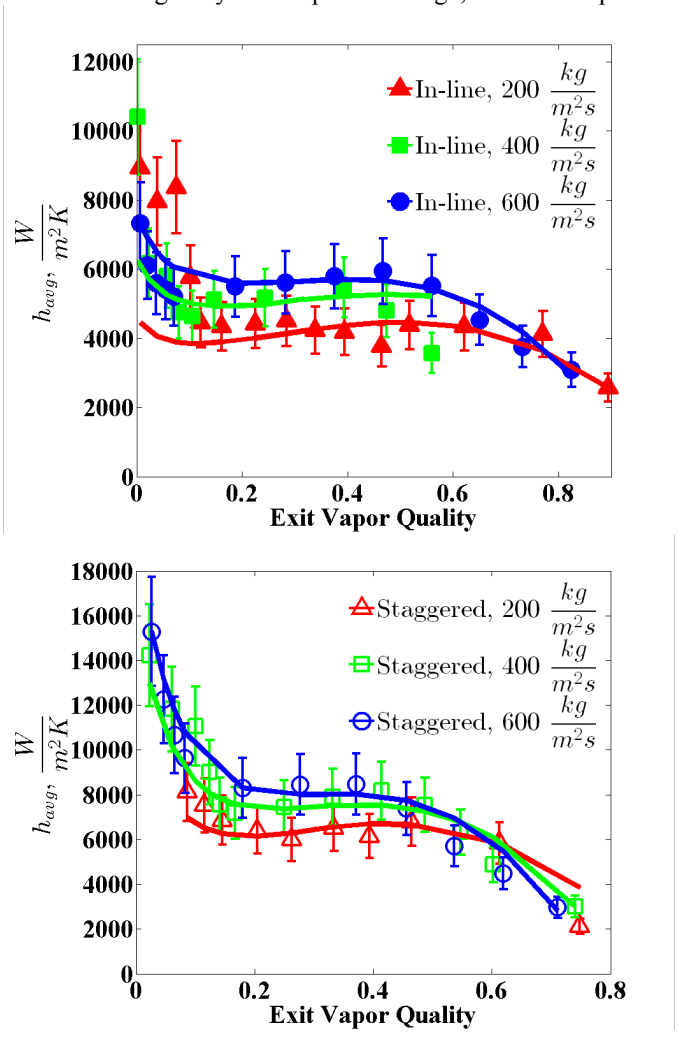

Figure 14: New two phase heat transfer coefficient correlation prediction for HFE-7200 in the inline array (top) and staggered array (bottom)

heat sinks at laminar Reynolds numbers less than 10^3. Since good prediction accuracy for the current single phase data was obtained with the Tullius et al. Nusselt number correlation using optimized shape factors in Chapter 3, these will be used in place of the Short et al. relation.

Next, the constant ζ=1 correction factor for the average heat transfer coefficient, will instead be replaced by an enhancement equation with exit quality and mass flux dependence. The equation will have 5 variable constants, C_1, C_2, C_3, C_4, and C_5. This will facilitate generation of the final correlation for average heat transfer coefficient by allowing adjustment of the shape of the curve for both pin fin arrays over the entire range of exit quality. The form of the equation will be: $\zeta = C_1 e^{C_2 x_e} + C_3 x_e^3 + \left(\frac{C_4}{G + C_5} \right)^{1/2}$

The form of this equation has a quality dependent exponential function in the first term, an exit quality dependent cubic function in the second term, and a mass flux dependent function in the third and final term.

After using this new two phase equation and selecting the constants C_1 – C_5 that minimize MAE for both arrays, the resulting prediction curves for deionized water are shown in Figure 13. Since the experimental water heat transfer coefficients for the inline and staggered arrays were nearly the same, one set of constants were used to generate the equation. A remarkably small MAE of 2.44% was obtained overall for water.

For HFE-7200, two sets of constants were optimized separately, each for the inline and staggered arrays. The prediction curves are shown in Figure 14. An MAE of 13.16% was obtained for the inline array and an MAE of 10.18% was obtained for the staggered array. A summary of the new correlation along with the constants used is given in Table 1.

Table 1: New Heat Transfer Coefficient Correlation Summary

Fluid	Array	C_{Nu}	C_1-C_5	MAE
Water	Inline	0.0495	C_1= -0.07 C_2=4.3 C_3= 0 C_4=80 C_5=2965	2.44%
Water	Staggered	0.0413	C_1= -0.07 C_2=4.3 C_3= 0 C_4=80 C_5=2965	2.44%
HFE-7200	Inline	0.054	C_1= 2.47 C_2=-9.2 C_3= -1.71 C_4=45 C_5=181	13.16%
HFE-7200	Staggered	0.065	C_1= 6.0 C_2= -14.15 C_3= -3.63 C_4=45 C_5=88	10.18%

Time variation of heat flux: Experiments under condition of time-varying heat flux were carried out, once again using the test section from [13] at two values of mass flux m= 230 kg/m^{2}s and m= 380 kg/m^{2}s. The lowest heat flux was applied to maintain the steady state heated wall temperature in the

range T_W= ± 2 ^{0}C. Then, during a time interval of 9-10s, we increased the heat flux linearly with respect to time until the heated wall temperature was within of a few degrees of T_W= 50 ^{0}C. Data sets were recorded and averaged. Figures 15a and 15b show time variation of heat flux at m= 230 kg/m^{2}s and m=380 kg/m^{2}s, respectively. The deviation of the measurements from the straight line cannot be distinguished within the uncertainty range.

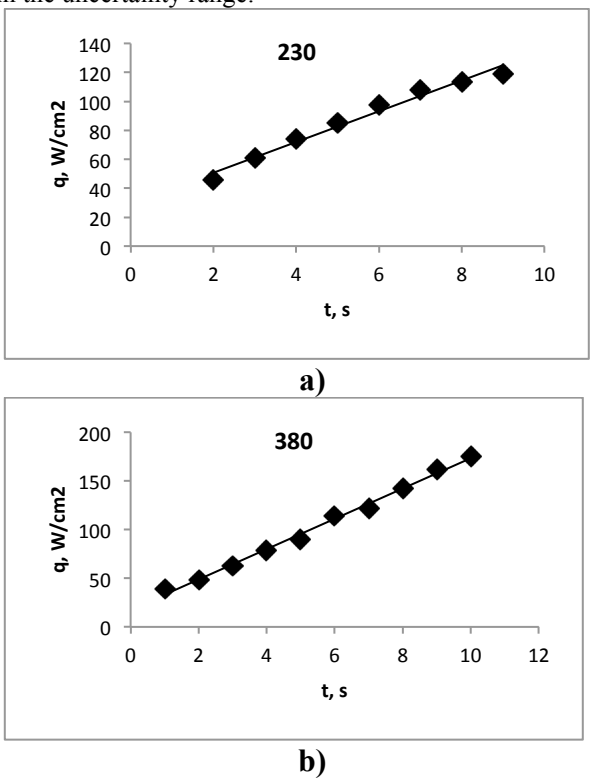

Figure 15: Time variation of heat flux

Time variation of average heated wall temperature: One of the most important parameters of the heat sink is the temperature of the heated wall, $T_{W,}$ often called the base temperature. The base temperature in electronic packaging is the reference temperature for all the electronic components attached to the base. Using this reference temperature one can estimate the maximum junction temperatures and decide if a given component may be employed. Figures 16a and 16b illustrate the time variation of the average heated wall temperature at m=230 kg/m^{2}s and m=380 kg/m^{2}s, respectively. The heat flux varied

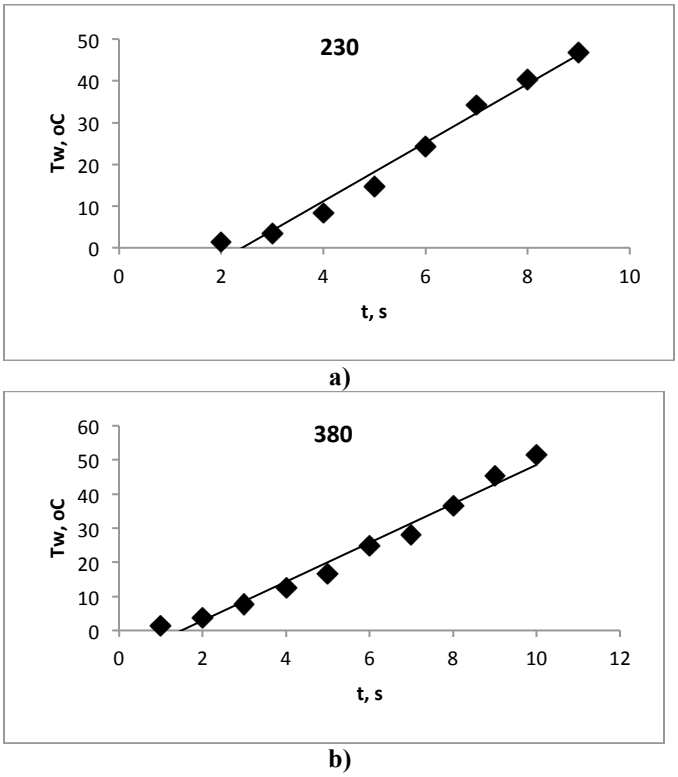

Figure 16: Time variation of temperature on the heated surface

according Figs. 15a, b. The wall temperature increases with time up to 46.8 ^{0}C at m=230 kg/m^{2}s and up to 51.6 ^{0}C at m=380 kg/m^{2}s. It may be concluded that for known heat sink mass and capacity and known time variation of heat flux, the value of mass flux may be chosen to keep the maximum reference temperature within a given range.

Boiling parameters under temporal variations of heat flux: Figure 17 shows the temperature field and histogram at fixed time instant of 10 s, and q_{max}= 170 W/cm^2, m=380 kg/m^{2}s. The time and surface averaged wall temperature is 51.6 ^{0}C, the maximum deviation from the average value does not exceed ± 2 ^{0}C. This value does not differ significantly from the value of ± 1.5 ^{0}C obtained under steady state condition.

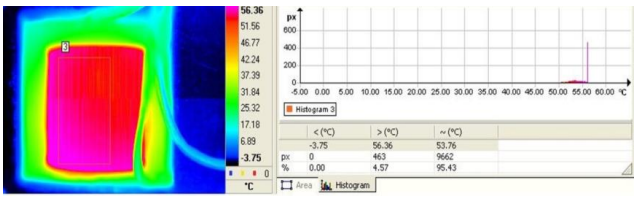

Figure 17: Temperature field on the heater

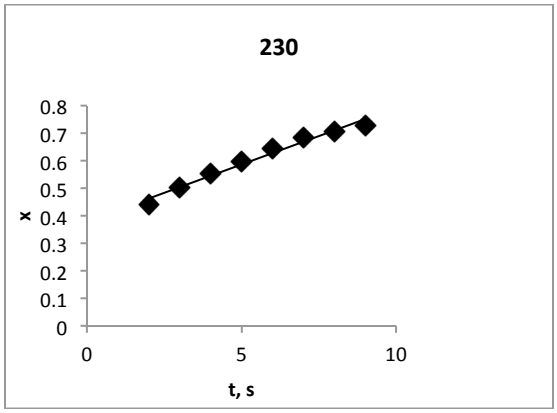

a)

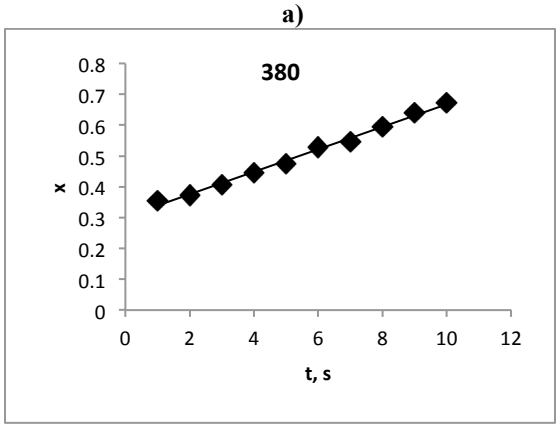

b)

Figure 18: Time variation of vapor quality

Figure 18 shows time variation of vapor quality at the outlet of text section. Figures 16a and 16b show the variation of the heat transfer coefficient with vapor quality at the outlet of the test section for different values of heat flux. This quality was varied experimentally by linearly increasing heat flux during time of 9-10 s, while maintaining a constant mass flux. Figures 19a, b show that up to vapor quality of about x=0.55 the heat transfer coefficient increases with increasing vapor quality.

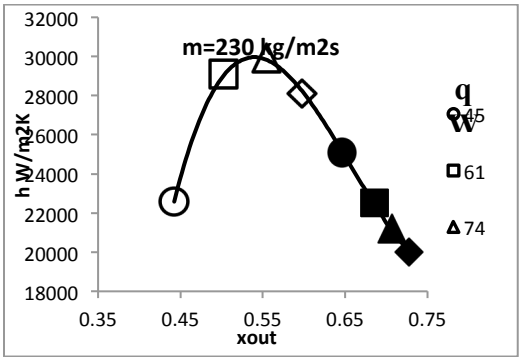

a)

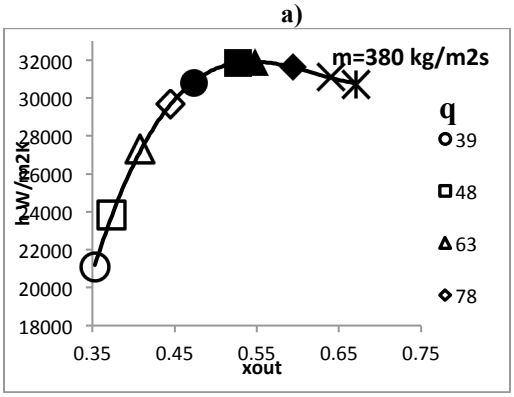

b)

Figure 19: Dependence of heat transfer coefficient on vapor quality

When the vapor quality exceeds the value of x> 0.55 the heat transfer coefficient decreases with increasing vapor quality. Such a behavior agrees with results reported above. Another noteworthy feature of the same data is the larger magnitude of the heat transfer coefficients compared to values obtained under steady state conditions. Under transient conditions the dissipated power is absorbed not only by the working fluid but partially it is also adsorbed by material of heat sink. For example, at m=380 kg/m^{2}s and q_{max}=170 W/cm^2 the heat transfer coefficient was 25000 and 31000 W/m^{2}K for steady-state and time varying conditions, respectively.

LEAST MATERIAL AND LEAST ENERGY ANALYSIS FOR CPV COOLING

The Coefficient of Performance (COP) is traditionally used to describe the cooling capability or heat output of a thermodynamic system in relation to the electrical or mechanical energy used to drive the cooling or heating process and serves as a basis of comparison for heat pump and refrigeration equipment. It is expressed as $COP = \frac{Q}{W}$ where Q is the heating energy or cooling output (kWh) and W is the energy input (kWh).

With a modest re-definition, this metric can also be applied to actively cooled CPV cells, taking the ratio of the useful electrical power generated by the cell (solar energy harvest or net solar energy) to the power consumed by the

pump to cool the cell. The equation for COP used in this way will be given as:

$$COP = \frac{E_{PV} - P_{Pump}}{P_{Pump}} = \frac{\text{Solar Energy Harvest}}{\text{Pumping Power}} \qquad (6)$$

This equation depends only on solar energy and pumping power and does not include energy from other sources. However, it could be modified to include other parasitic losses e.g. transmission line loss and power for the control electronics. In addition to the pumping power and parasitic losses, account should also be taken of the energy associated with the mining and refining of the raw materials, as well as the manufacture, transportation and final assembly of all the various components and materials in a CPV system. Such an extensive energy analysis, cataloging, quantifying, and optimizing the energy content for each of these processes for all the components, is beyond the scope of the present effort. Instead, this study will limit its attention to the embedded energy in the micro-cooler material and the required pumping power**.**

The total mass of the copper used in the fabrication of the micro-cooler determines the embedded energy content and has a direct impact on the performance of the cooling system. The material mass has associated formation energy for processing the copper and additional energy is required for the further refinement or "fabrication" of that raw metal into its final form. Ashby [15] found that 27 kWh/kg is the value of embodied energy for copper taking into account material, processing and recycling energy.

In the COP of Equation 6, we will add the embedded energy to the pumping power in the denominator and convert the power terms to work terms by multiplying by the total lifetime hours of operation, t_L. The result is a Total Coefficient of Performance (COP_T) metric defined as:

$$COP_T = COP\left(\frac{P_{pump}t_L}{P_{pump}t_L + 27000m}\right) = \frac{\text{Solar Energy Harvest} \cdot \text{Lifetime Hours}}{\text{Pumping Work + Embodied Energy}} \qquad (7)$$

Although the COP_T metric was derived from the COP, it is distinct in that embedded energy is included to account for the energy required for the formation and fabrication of the copper as well as the lifetime energy of the pump. In addition, since multi-junction cells are expected to last 25 years or more in a stable environment, and the solar industry is under pressure to increase cell lifetime to at least 30 years, in this analysis total lifetime t_L will be taken as 30 years assuming CPV operation for an average of 12 hours per day. It will be shown that COP and COP_T can be useful metrics to aid in identifying the system geometry that allows the most efficient use of mass and pumping power, while maintaining good cooling performance and high solar cell efficiency. Finally, it should be noted that the COP and COP_T are indirectly dependent on

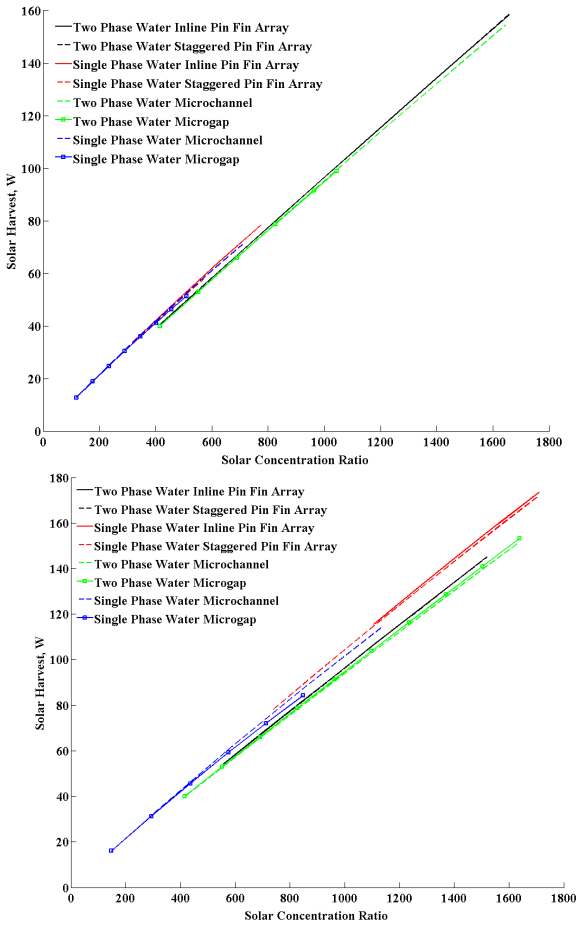

Figure 20: Solar Energy Harvest for a constant mass flow rate of 33 g/min (top) and 70 g/min (bottom). Solar heat flux range from 20 W/cm^2 – 165 W/cm^2.

system parameters such as the fin geometry, flow rate, solar concentration etc.

For the forthcoming analysis a cell aperture area equivalent to the 28.8mm x 9.6mm base area of the pin fin coolers will be assumed. This is a valid assumption since Spectrolab 40% efficient, triple junction CPV cells are available in multiple sizes, as small as 5.5mm x 5.5mm. Therefore the 28.8mm x 9.6mm area could be considered as a cooling "module" of 3 or more CPV cells, which could then be used with other modules in a theoretical two phase manifold cooling system. This concept is similar to the Solar Systems single phase liquid cooling manifold design as described previously.

To round out the comparison, longitudinal-finned microchannels of similar geometry and aspect ratio to the inline pin fin array, and a microgap cooler will be included in the model. A single channel microgap cooler is included in this comparison due to being the best of the longitudinal channels as found in [16]. The microchannel cooler will have 31 channels with the same channel width and height of 153μm and 305μm respectively. The microgap cooler will have 1mm thick walls and a 1mm thick base with a channel height of

305µm. All coolers are assumed to have the same 1mm thick base wall, along with a 50µm layer of 63% Sn/37% Pb solder as the cell's thermal interface material. Working fluid for all simulations will be water.

Figure 20 is the solar energy harvest, which is the total power generated by the theoretical Spectrolab triple junction CPV module, minus pumping power, for a heat flux range from 20 W/cm^2 – 165 W/cm^2. Embodied energy is not included in the solar harvest analysis or Figure 20. A constant flow rate of 33 g/min for the top plot, and 70 g/min for the bottom plot of Figure 20 is assumed for each cooler in each of the respective plots. It is easy to see upon inspection of both plots that the pin fin energy harvest is better for the pin fin arrays than the microchannel and microgap coolers by 1 to 10 watts, depending on the concentration ratio and flow rate. The difference between the inline and staggered arrays ranges from less than 1 watt to 1 watt with the inline array having a slight advantage in solar harvest.

For the low flow rate in the top plot of Figure 20, the single phase microchannel, the single phase pin fin coolers and single phase microgap cooler are not able to provide cooling above 800 suns. Also the two phase microgap cooler cannot provide cooling above 1100 suns due to reaching CHF above this point. Further, both of the two phase pin fin coolers, which are able to provide cooling to over 1600 suns, will generate 160 watts of usable power for our theoretical CPV module.

Shifting attention to the bottom of Figure 20 we can see that the pin fin arrays still facilitate the best solar power generation by the CPV module. However, due to the high flow rates in this case the single phase pin fins are able to provide lower average base temperature and thus generate 10 more watts than the two phase pin fin coolers at an eqivalent concentration of 1500 suns.

The COP_T, which is defined in Equation 7, is shown in Figure 21 and includes the embodied energy of the copper microcooler. The highest COP_T of 8 x10^4 is obtained by the single phase microgap at 500 suns, which sharply increases up to this maximum value due to constant single phase pumping power over increasing insolation. The two phase cooling devices COP_T, however, are generally more constant. In the range shown, the two phase pin fin coolers stay near 10^4 over the entire range and are the most energy efficient microcooler for cooling above 1000 suns. In the bottom plot of Figure 12, COP_T is substantially lower for all arrays due to the higher flow rate and thus higher pumping power. Once again the inline single phase pin fins provide the best cooling, even up to 1700 suns, but does so only at a higher flow rate. Thus, at these higher heat fluxes or insolations above 1000 suns, the COP_T is higher - and therefore more energy efficient - when utilizing lower flow rate two phase pin fin cooling.

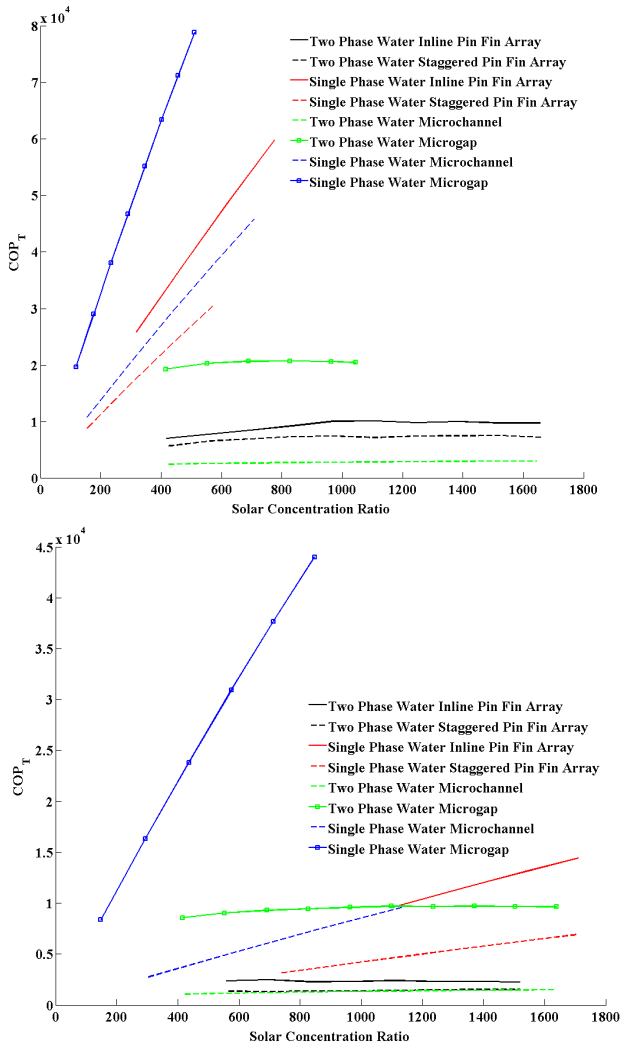

Figure 21: COP_T for a constant mass flow rate of 33 g/min (top) and 70 g/min (bottom). Solar heat flux range from 20 W/cm^2 – 165 W/cm^2.

CONCLUSION

(1) Three unique micro pin fin arrays – staggered and inline – all of similar geometric proportion, were experimentally investigated in single and two phase flows for both deionized water and HFE-7200 working fluids up to exit qualities of 90%.

(2) Single phase and two phase heat transfer coefficient behavior between water and HFE-7200 significantly differed over exit quality, with a distinctly increasing trend for water and a more 'M' shaped curve for HFE-7200. We think it is reasonable to assume that the lower surface tension, lower liquid-vapor density ratio, and lower latent heat of HFE-7200 compared to water could play a significant role in the differing behavior of the two fluids in inline vs staggered pin fin arrays.

(3) Both single phase and two phase cooling can act as efficient CPV thermal management techniques

however two phase provides a distinct advantage over single phase in terms of heat transfer coefficient.

(4) For high heat fluxes encountered at 1000 suns, and higher for high solar power generation at low flow rates, two phase micro pin fins are the most energy efficient design for CPV cooling systems. For high flow rates and high heat flux cooling, single phase pin fins provide the most energy efficient design choice. For low heat flux encountered at low concentration ratio, single phase microgap maintains lower cell temperatures for the lowest parasitic pumping penalty. For both single phase and two phase cooling, inline pin fin arrays are generally more energy efficient than staggered arrays.

(5) A technique for thermal visualization and determination of spatially resolved time series of wall temperature during flow boiling in a pin-fin micro-channel heat sink was presented. The results of quantitative measurements, such as deviations of the surface temperature from time and space average values, are discussed. Results show that temperatures can be maintained with an uncertainty varying from 1.5 ^{o}C at q=30 W/cm^2 to 2.0 ^{o}C at q= 170 W/cm^2. These results indicate that pin-fin micro-channel heat sink enables to keep an electronic device near uniform temperature under conditions of steady state and time varying high heat fluxes.

(6) The heat transfer coefficient varied significantly with refrigerant quality and showed a peak at a vapor quality of 0.55 in all the experiments. At relatively low heat fluxes and vapor qualities the heat transfer coefficient increased with vapor quality. At high heat fluxes and vapor qualities the heat transfer coefficient decreased with vapor quality. Noteworthy feature of the same data is the higher heat transfer coefficients attained under transient conditions, compared to values obtained under steady state conditions.

REFERENCES

[1] NREL, "Cell Efficieny Chart," October 2014. [Online]. Available: http://www.nrel.gov/ncpv/images/efficiency_chart.jpg.

[2] N. Yastrebova, "High-efficiency multi-junction solar cells: current status and future potential," 2007.

[3] S. H. Antonio Luque, Handbook of photovoltaic science and engineering, West Sussex: John Wiley & Sons Ltd, 2011.

[4] G. M. D. R. R. P. S. D. Landis, "High-temperature solar cell development," 2005.

[5] Spectrolab, [Online]. Available: http://www.spectrolab.com/DataSheets/PV/CPV/C4MJ_40Percent_Solar_Cell.pdf .

[6] K. E. Y. H. W. W. E. D. Martin Green, "Solar cell efficiency tables," *Progress in Photovoltaics,* vol. 20, no. 1, pp. 12-20, 2012.

[7] P. Verlinden, A. Lewandowski, H. Kendall, S. Carter, K. Cheah, I. Varfolomeev, D. Watts, M. Volk, I. Thomas, P. Wakeman, A. Neumann, P. Gizinski, D. Modra, D. Turner and J. Lasich, "Update on two-year performance of 120 kWp concentrator PV systems using multi-unction III-V solar cells and parabolic dish reflective optics," in *Photovoltaic Specialists Conference*, 2008.

[8] T. Ho, "Improving efficiency of high-concentrator photovoltaics by cooling with two-phase forced convection," *International journal of energy research,* vol. 34.14, pp. 1257-1271, 2010.

[9] T. T. Y. B. J. Tullius, "Optimization of short micro pin fins in minichannels," *International Journal of Heat and Mass Transfer,* vol. 55, pp. 3921-3932, 2012.

[10] Y. P. S. Krishnamurthy, "Flow boiling of water in a circular staggered micro-pin fin heat sink," *International Journal of Heat and Mass Transfer,* vol. 51, pp. 1349-1364, 2008.

[11] A. S.-H. W. Qu, "Experimental study of saturated boiling heat transfer in an array of staggered micro pin fins," *International Journal of Heat and Mass Transfer,* vol. 52, 2009.

[12] A. R. P. K. P. B. D. McNeil, "A comparison of flow boiling heat transfer in in-line mini pin fin and plane channel flows," *Applied thermal engienering,* vol. 30.16, pp. 2412-2425, 2010.

[13] D. M. A. M. A. B.-C. G. H. T. David, "Thermal management of time-varying high heat flux electronic devices," *J. Electron. Packag.,* vol. 136, no. 2, 2014.

[14] R. R. J. T. A. B.-C. E. Rahim, "Characterization and prediction of two phase flow regimes in minature tubes," *International Journal of Multiphase Flow,* vol. 37, pp. 12-23, 2011.

[15] M. Ashby, Materials and the Environment: Eco-Informed Material Choice, Butterworth-Heinemann, 2009.

[16] P. W. G. H. A. B.-C. Alexander Reeser, "Energy efficient two-phase microcooler design for a concentrated photovoltaic triple junction cell," *Journal of Solar Energy Engineering,* vol. 136, no. 3, pp. 03015-1:11, 2014.

[17] A. Reeser, "Energy efficient two phase cooling for concentrated photovoltaic arrays," Graduate Thesis, College Park, 2013.